HHS Public Access

Author manuscript

Macromol Biosci. Author manuscript; available in PMC 2020 January 01.

Published in final edited form as:

Macromol Biosci. 2019 January ; 19(1): e1800248. doi:10.1002/mabi.201800248.

Injectable supramolecular hydrogel/microgel composites for therapeutic delivery

Minna H. Chen,
Department of Bioengineering, University of Pennsylvania, 210 S 33rd St, Philadelphia, Pennsylvania, 19104, USA

Dr. Jennifer J. Chung,
Division of Cardiovascular Surgery, Department of Surgery, University of Pennsylvania, Silverstein 6, 3400 Spruce St, Philadelphia, Pennsylvania, 19104, USA

Joshua E. Mealy,
Department of Bioengineering, University of Pennsylvania, 210 S 33rd St, Philadelphia, Pennsylvania, 19104, USA

Samir Zaman,
Division of Cardiovascular Surgery, Department of Surgery, University of Pennsylvania, Silverstein 6, 3400 Spruce St, Philadelphia, Pennsylvania, 19104, USA

Elizabeth C. Li,
Division of Cardiovascular Surgery, Department of Surgery, University of Pennsylvania, Silverstein 6, 3400 Spruce St, Philadelphia, Pennsylvania, 19104, USA

Maria F. Arisi,
Division of Cardiovascular Surgery, Department of Surgery, University of Pennsylvania, Silverstein 6, 3400 Spruce St, Philadelphia, Pennsylvania, 19104, USA

Prof. Pavan Atluri, and
Division of Cardiovascular Surgery, Department of Surgery, University of Pennsylvania, Silverstein 6, 3400 Spruce St, Philadelphia, Pennsylvania, 19104, USA

Prof. Jason A. Burdick
Department of Bioengineering, University of Pennsylvania, 210 S 33rd St, Philadelphia, Pennsylvania, 19104, USA, burdick2@seas.upenn.edu

Abstract

Shear-thinning hydrogels are useful for biomedical applications, from 3D bioprinting to injectable biomaterials. Although they have the appropriate properties for injection, it may be advantageous to decouple injectability from the controlled release of encapsulated therapeutics. Toward this, composites of hydrogels and encapsulated microgels are introduced with microgels that are fabricated via microfluidics. The microgel crosslinker controls degradation and entrapped molecule release, and the concentration of microgels alters composite hydrogel rheological

Supporting Information
Supporting Information is available from the Wiley Online Library or from the author.

properties. For treatment of myocardial infarction (MI), interleukin-10 (IL-10) is encapsulated in microgels and released from composites. In a rat model of MI, composites with IL-10 reduce macrophage density after 1 week and improve scar thickness, ejection fraction, cardiac output, and the size of vascular structures after 4 weeks when compared to saline injection. Improvements are also observed with the composite without IL-10 over saline, emphasizing the role of injectable hydrogels alone on tissue repair.

Graphical Abstract

Guest-host hyaluronic acid hydrogels are combined with covalently-crosslinked hyaluronic acid microgels with encapsulated therapeutics to create composites that are injectable and can deliver therapeutics with controlled release kinetics. Here, feasibility is demonstrated using composite hydrogels to deliver interleukin-10 in a rat MI model.

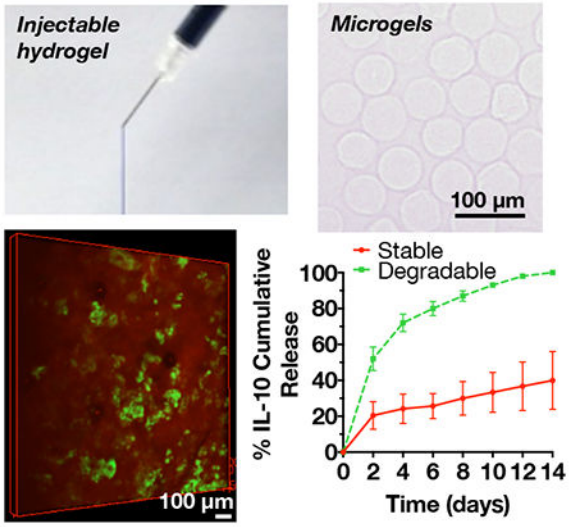

Keywords

supramolecular; hydrogels; microgels; composites; drug delivery

1. Introduction

Hydrogels are being developed for a wide range of biomedical applications, due to the diverse properties that are possible with hydrogel design[1]. Supramolecular hydrogels represent a specific class of hydrogels with reversible, non-covalent crosslinks that permit injectability[2–4]. Examples of supramolecular chemistry include molecular self-assembly[5–8], host-guest complexes[9–11], and mechanically-interlocked molecular structures[12]. Supramolecular hydrogels have been used in a variety of biomedical applications, including but not limited to imaging[13,14], tissue engineering[6,15,16], and therapeutic delivery[17,18]. The injectable nature of supramolecular hydrogels makes them particularly attractive for clinical translation since they can be delivered using minimally invasive approaches.

Strategies for therapeutic delivery from supramolecular hydrogels include the direct encapsulation of growth factors or cells[19–21], which may contain enzymatically or hydrolytically degradable crosslinks to control release[22]. Interactions between small molecules and components of the supramolecular complex can also be used to sequester cargo and control molecule release[23]. Additionally, nanoparticles can be assembled into networks through interactions with polymers to deliver therapeutics[24]. In this way, molecule release can be controlled through nanoparticle design, allowing for extended release over direct encapsulation in a hydrogel.

Injectable hydrogels are of particular interest in the treatment of tissue after myocardial infarction (MI)[25,26]. Almost 800,000 Americans each year suffer from a heart attack or MI, which occurs when an occlusion in a coronary artery causes inadequate blood flow to the heart[27]. Depending on the severity of MI, adverse remodeling can lead to significant decreases in cardiovascular function and heart failure (HF)[28]. HF affects almost 5.7 million Americans and has a 50% mortality rate within 5 years[29]. Current medical and surgical treatments aim to improve the quality and length of life for patients with HF, but are primarily targeted to the tissue after remodeling. Thus, a clinical need exists to develop a therapy for ischemic MI that can attenuate remodeling and resulting tissue damage.

Numerous hydrogel therapies have been developed that can improve tissue properties after infarction[30,31]. In some cases, the hydrogel is used to directly thicken the ventricle wall in approaches that have been evaluated in preclinical studies and in US clinical trials[32,33]. According to the Law of Laplace, wall thickness is inversely proportional to wall stress, so thickening the left ventricle wall leads to reduced wall stress, preventing further wall thinning and ventricular dilation which can lead to decreased cardiac function[34,35]. In other approaches, hydrogels are used to deliver therapeutics (e.g. cells, drugs) to the tissue for a local and sustained response, with targets that include improved vascularization[20,36,37] and cardiomyocyte proliferation[38]. Specifically, shear-thinning hydrogels have been introduced alone and for therapeutic delivery to the heart, through direct injections from syringes to percutaneous delivery from catheters[26,35,39].

To utilize the benefits of supramolecular hydrogels for injectability and retention and to decouple the delivery of encapsulated therapeutics from the supramolecular hydrogel design, we demonstrate here the development and application of an injectable supramolecular hydrogel/microgel composite for localized and sustained therapeutic delivery. The supramolecular hydrogel is based on our previous work in which hyaluronic acid (HA) is modified separately with adamantane (guest) and ß-cyclodextrin (host) to form an injectable supramolecular hydrogel upon mixing[11] and the microgels are fabricated from covalently-crosslinked HA hydrogels using a high-throughput microfluidic device[40]. As a model therapeutic, we chose to deliver interleukin-10 (IL-10), an anti-inflammatory cytokine[41,42] to address excessive inflammation that can cause extensive damage to the myocardium after MI[42]. Although shown here to treat MI, such a composite hydrogel/microgel system could be used for the delivery of a wide range of therapeutics to treat numerous clinical indications.

2. Experimental Section

2.1. Materials

All chemicals were purchased from Sigma-Aldrich unless otherwise noted.

2.2. Material Synthesis

2.2.1. HA-TBA, AdHA, and CDHA—HA-TBA, adamantane-modified HA (AdHA), and ß-cyclodextrin-modified HA (CDHA) were synthesized as previously described[11]. For HA-TBA, sodium hyaluronic acid (HA, 74 kDa, Lifecore) was dissolved at 2% w/v in DI water and exchanged with Dowex 50W × 200 resin (3 g resin/1 g HA) for 2 hours at room temperature. The resin was filtered and then the solution was titrated to pH 7 with tetrabutylammonium hydroxide, frozen, and lyophilized.

For AdHA synthesis, HA-TBA was coupled to 1-adamantane acetic acid (Acros Organics) in the presence of di-tert-butyl dicarbonate and 4-methylaminopyridine in anhydrous dimethyl sulfoxide (DMSO) under nitrogen for 20 hours at 45°C. Reaction products were dialyzed for 2 weeks in DI water, filtered, frozen, and lyophilized. Functionalization of HA by adamantane was approximately 20% as quantified via ^{1}H NMR (Supplementary Figure 1A).

For fluorescent labeling, a standard solid phase peptide synthesizer (PS3, Gyros Protein Technologies) with glycinol 2-chlorotrityl resin was used to synthesize fluorescent peptides GCDDD-rhodamine B (for gel labeling) or GCDDD-5(6)-carboxyfluorescein (for microgel labeling). Peptides were cleaved from the resin using a solution of 95% trifluoroacetic acid, 2.5% triisopropylsilane, and 2.5% water, precipitated twice in cold diethyl ether, dissolved in water, frozen, and lyophilized before use. Peptide synthesis was confirmed using MALDI-TOF mass spectrometry. For gel visualization, AdHA was methacrylated (15% modification) via esterification with methacrylic anhydride (1 mL/1 g AdHA) at pH 8.5 for 3 hours, dialyzed for 3 days in DI water, filtered, frozen, and lyophilized to form AdMeHA. AdMeHA was dissolved at 2 mg/mL in triethanolamine buffer (0.2 M in PBS, pH 10) and reacted with fluorescent peptide (GCDDD-rhodamine B, 0.015 mol eq) for 2 hours at 4°C. Reaction products were dialyzed for 4 days at 4°C, frozen, and lyophilized to form AdMeHA-Rho.

For CDHA synthesis, ß-cyclodextrin (ß-CD) was conjugated with a hexane diamine linker to form ß-CD-HDA as previously described[11]. HA-TBA was coupled with ß-CD-HDA in the presence of benzotriazole-1-yl-oxy-tris-(dimethylamino)-phosphonium hexafluorophosphate (BOP) in anhydrous DMSO under nitrogen for 3 hours at room temperature. The reaction was quenched with cold DI water, dialyzed in the presence of NaCl for 3 days, dialyzed in DI water for 5 days, filtered, frozen, and lyophilized. Functionalization of HA by ß-cyclodextrin was approximately 20% as quantified via ^{1}H NMR (Supplementary Figure 1B).

2.2.2. NorHA—Norbornene-modified HA (NorHA) was synthesized as previously described[43]. Briefly, HA-TBA was coupled with 5-norbornene-2-methylamine (TCI Chemicals) in the presence of BOP in anhydrous DMSO under nitrogen for 2 hours at room temperature. The reaction was quenched with cold DI water, dialyzed in the presence of

NaCl for 3 days, dialyzed in DI water for 5–7 days, filtered, frozen, and lyophilized. Functionalization of HA by norbornene was approximately 30% as quantified via ^{1}H NMR (Supplementary Figure 1C).

2.2.3. HepSH—Thiolated heparin (HepSH) was synthesized based on previously described reports[44,45]. Briefly, heparin (5 mg/mL) was dissolved in DI water and reacted with cystamine-dihydrochloride (30 mol/mol heparin) in the presence of 1-ethyl-3-(3-dimethylaminopropyl)carbodiimide-HCl (EDC, 20 mol/mol heparin) and 1-hydroxybenzotriazole hydrate (HOBt, 20 mol/mol heparin) at pH 6.8 for 5 hours at room temperature. Reaction products were purified by dialysis for 3 days, frozen, and lyophilized, then re-reacted with tris (2-carboxyeethyl) phosphine-HCl (TCEP, 10 mol/mol heparin) to reduce oxidized disulfide groups at pH 7.5 for 3 hours at room temperature. After 3 hours, the pH was adjusted to 5.0 with 1.0 N HCl and the solution was dialyzed against dilute HCl (pH 3-3.5) with 100 mM NaCl for 3 days at 4°C and then without NaCl for an additional 4 days at 4°C. Reaction solution was aliquoted into 1.5 mL tubes, frozen, and lyophilized overnight. Percent conjugation of thiol groups to heparin was determined to be approximately 45% via Ellman assay.

2.3. Microgel Formation and Characterization

2.3.1. Microgel Formation—Microgels were formed via water-in-oil emulsion using a microfluidic device with parallel flow-focusing particle generators as previously described[40,46]. The aqueous phase (1 mL) consisted of NorHA (30 mg, 3% w/v), thiol crosslinker (pentaerythritol tetrakis(mercaptoacetate), PETMA, TCI Chemicals or 1,4-dithiothreitol (DTT)) at 0.95 mol thiol per 1 mol norbornene, Irgacure-2959 (I2959, 0.05% w/v), HepSH (0.05 mol thiol per 1 mol norbornene), and (if indicated) rat IL-10 (R&D Systems, 12 μg) and was attached to an in-line 0.22 μm filter with a flow rate of 0.6 mL/hr. For visualization purposes, if indicated, fluorescein isothiocyanate-dextran (FITC-dextran, 2 MDa, 1 mg) or fluorescent peptide (GCDDD-5(6)-carboxyfluorescein, 0.05 mol thiol per 1 mol norbornene) was incorporated in the aqueous solution. The oil phase consisted of 2% w/w Span 80 in mineral oil and was filtered using a 0.45 μm filter prior to use at a flow rate of 3.5 mL/hr. Microgels were crosslinked via UV light (OmniCure Series 1500, Excelitas, 320–390 nm, 20 mW/cm^2) as they flowed out of the device and into a collection vial. Microgels were washed with water and then isopropanol to remove oil, dried overnight on vacuum, and stored at −20°C.

2.3.2. IL-10 Encapsulation Efficiency and Zeta Potential—Microgels loaded with IL-10 and crosslinked with PETMA were formed either with (n=3) or without HepSH (n=3) to determine the effect of heparin on IL-10 sequestration. Heparin has a high negative charge density that can attract positively charged cytokines such as IL-10. Following microgel formation, microgels were rehydrated at 1 mg microgel/1 mL release buffer with hyaluronidase (1 mg/mL). After microgels were fully degraded at 48 hours, IL-10 content was quantified via ELISA (DuoSet kit, R&D Systems) and encapsulation efficiency was determined as the ratio of the detected amount of IL-10 to the expected amount of IL-10.

For zeta potential measurements, solutions of NorHA (1 mg/mL in filtered water, pH 8) and NorHA with HepSH (0.05 mol thiol per 1 mol norbornene, pH 8) were prepared and the zeta potential of these microgel precursor solutions was measured using a Zetasizer Nano ZS90 (Malvern Panalytical) at 25°C.

2.3.3. Characterization of Microgel Size, Degradation, and IL-10 Release—To characterize size, microgels were rehydrated in PBS and imaged at 10x using brightfield microscopy. The straight line tool in ImageJ (NIH) was used to measure microgel diameters (n=22). For degradation and release quantification, microgels loaded with IL-10 and crosslinked with either a stable (DTT, n=3) or degradable (PETMA, n=3) crosslinker were rehydrated in release buffer (1% bovine serum albumin in PBS) at 1 mg microgel/1 mL release buffer and washed via centrifugation at 1200 × *g* for 15 minutes. Release buffer was replaced and collected every other day and stored at −20°C. After 2 weeks, microgel samples were fully degraded in hyaluronidase (1 mg/mL). HA release was determined using an uronic acid assay and IL-10 release was quantified via ELISA (DuoSet kit, R&D Systems).

2.4. Composite Hydrogel Formation and Characterization

2.4.1. Composite Hydrogel Formation—Bulk guest-host hydrogel (4% w/w, 1 mol Ad: 1 mol CD) and degradable microgels (low concentration: 6.7 mg/mL bulk hydrogel or high concentration: 13.3 mg/mL bulk hydrogel) were combined to form a composite hydrogel. Guest-host hydrogel materials (AdHA and CDHA) and microgels were weighed and CDHA was combined with microgels in the same microcentrifuge tube. Following sterilization with a germicidal lamp (40 minutes; turn materials at 20 minutes), hydrogel components were dissolved in sterile PBS. To mix, the AdHA solution was added to the CDHA/microgel solution with a pipette. For rheology samples, hydrogels were further sonicated at 60°C for 10 minutes, vortexed, and centrifuged to promote more homogeneous mixing and to remove air bubbles. Using a scoopula, the composite hydrogel was loaded either onto the rheometer or into 27G × ½” insulin syringes (BD) for animal studies.

2.4.2. Volume Fraction of Microgels in Composite Hydrogel—Composite hydrogels were prepared as described above using rhodamine-labeled bulk guest-host hydrogel components (AdMeHA-Rho) and fluorescein-labeled microgels at both low (6.7 mg/mL bulk hydrogel) and high (13.3 mg/mL bulk hydrogel) concentrations. Confocal microscopy was used to image the composite hydrogel and the 3D Viewer plugin (ImageJ, NIH) was utilized to create a 3D projection of the composite hydrogel. For each composite hydrogel image stack, regions of interest were selected and smoothed and a binary mask was created for each stack using an appropriate thresholding method in ImageJ. The 3D Objects Counter plugin (ImageJ, NIH) was used to determine the volume of objects in each image stack, and these volumes were combined to determine the volume fraction of microgels in the composite hydrogel.

2.4.3. Rheological Characterization—Oscillatory shear rheometry was used to characterize the material properties of the bulk hydrogel alone and of the composite hydrogels with low and high microgel concentrations. Hydrogels were prepared as described

above, and rheometer experiments were conducted as previously described[47] with a flat plate geometry and a gap size of 600 μm (10 times average microgel diameter). Briefly, time sweep (0.2% strain, 10 Hz), frequency sweep (0.01 to 100 Hz, 0.2% strain), strain sweep (0.01% to 500% strain, 10 Hz), continuous flow (shear rates from 0 s^{-1} to 50 s^{-1} over 2 min 30 sec), and cyclic strain (low: 0.2% strain, high: 500% strain, 10 Hz) experiments were completed for all samples (300 μL) at 25°C.

2.4.4. IL-10 Release—Composite hydrogels were formed with a high concentration of degradable microgels (50 μL bulk gel, n=3) and release buffer (1% bovine serum albumin in PBS) was added at 50 μL bulk gel/1 mL release buffer. Every other day, release buffer was collected via centrifugation at 1200 × *g* for 15 minutes, replaced, and stored at −20°C. After 2 weeks, composite hydrogels were fully degraded in hyaluronidase (1 mg/mL) and IL-10 release was quantified via ELISA (DuoSet kit, R&D Systems).

2.5. Rat MI Model

2.5.1. Infarct Induction and Hydrogel Injection—Using a previously established protocol, a left lateral thoracotomy in the fourth intercostal space was performed to allow for ligation of the left anterior descending artery to induce an infarct of approximately 30% of the left ventricle in a rat[20,47]. Animals were randomly assigned to one of three treatment groups: PBS (saline control), without IL-10 (composite hydrogel with high concentration of microgels without IL-10), and with IL-10 (composite hydrogel with high concentration of microgels with IL-10). PBS and composite hydrogels were loaded into 27G × ½” insulin syringes (BD) and delivered to the infarct in the border zone region in approximately 5 × 20 μL equally spaced injections. Animals were recovered and evaluated at either 1 week or 4 week timepoints. Prior to explant at 4 weeks, cardiac function was assessed using a 12-mm pressure-volume loop catheter (Millar). Following explant at 1 or 4 weeks, hearts were washed in PBS, and frozen in O.C.T. Compound (Tissue-Tek) at −80°C. From the apex to above the papillary muscles, tissue sections of 10 μm thickness were obtained using a cryostat. Animal procedures were approved by the University of Pennsylvania Institutional Animal Care and Use Committee.

2.5.2. Immune Response—After 1 week, immune response was assessed via immunohistochemical staining of tissue sections at the mid-papillary level for CD68 (MCA341GA, Bio-Rad, 1:500) with goat anti-mouse AF647 secondary (ab150115, Abcam, 1:300) and DAPI (D1306, ThermoFisher Scientific, 1:1000). Images were acquired on a Leica DM5000b fluorescent microscope using a DFC350 FX monochrome camera. At least 4 images of the border zone of the infarct, defined as one high-powered field away from the infarct, were quantified and averaged per animal for one biological replicate.

CD68 positive area fraction was quantified using ImageJ (NIH). A region of interest was selected for each image that included the tissue area only and excluded the composite hydrogel if applicable to assess immune response only in the surrounding tissue. Composite hydrogel areas were defined by large regions of sparse DAPI staining. A binary mask was created using the default thresholding method and then the area fraction of $CD68^+$ staining was measured for each image.

2.5.3. Tissue Remodeling—After 4 weeks, tissue remodeling was evaluated by staining tissue sections at the mid-papillary level with Masson's Trichrome Stain Kit using manufacturer provided instructions. Scar fraction was quantified using the freehand line tool in ImageJ (NIH) to measure the endocardial circumference of the left ventricle, the epicardial circumference of the left ventricle, the length of the endocardial infarct, and the length of the epicardial infarct, with "infarct" defined by portions of the left ventricular wall in which at least 50% of the thickness of the wall is scar. The scar fraction was calculated as follows:

$$Scar\ fraction = \frac{\frac{epicardial\ infarct}{epicardial\ circumference} + \frac{endocardial\ infarct}{endocardial\ circumference}}{2}$$

For scar thickness, the same tool was used to measure the width of 5 evenly spaced points of the infarct and averaged. At least 2 images were quantified and averaged per animal for one biological replicate.

2.5.4. Vascular Structures—After 4 weeks, vascular structure density and size were assessed via immunohistochemical staining of tissue sections at the mid-papillary level for von Willebrand factor (vWF-FITC, ab8822, Abcam, 1:400) and α-smooth muscle actin (α-SMA-AF594, ab202368, Abcam, 1:400) with wheat germ agglutinin (WGA-AF647, W32466, ThermoFisher Scientific, 1:300) and DAPI (D1306, ThermoFisher Scientific, 1:1000). Images were acquired on a Leica DM5000b fluorescent microscope using a DFC350 FX monochrome camera. At least four images of the border zone of the infarct, defined as one high-powered field away from WGA-bright scar, were quantified and averaged per animal to represent one biological replicate.

vWF^+ area and $vWF^+\alpha\text{-}SMA^+$ structure size was determined using ImageJ (NIH). For vWF^+ structures and $\alpha\text{-}SMA^+$ structures, a binary mask was created via thresholding. Thresholded images were processed with the Dilate and Erode functions to improve connectivity. Particles greater than or equal to 3.5 μm^2 in area were counted and measured. The Otsu auto-thresholding method was used unless 1) the area fraction of particles counted was greater than 10% or 2) the number of structures counted was over 200 for vWF^+ or 75 for $\alpha\text{-}SMA^+$. These cases were empirically determined to be indications that the Otsu auto-thresholding method was unsatisfactory; in these cases, the Triangle auto-thresholding method was used instead. For the number and size of $vWF^+\alpha\text{-}SMA^+$ structures, the result of using the AND operator in the Image Calculator function on the binary masks of the vWF and α-SMA channels was counted and measured using the parameters described above.

2.6. Statistics

All graphs and statistical analyses were completed using GraphPad Prism 7 software. Outliers were removed using the ROUT test with Q=5% and statistical significance was determined using a two-tailed Student's T-test or a one-way ANOVA with post-hoc Tukey's multiple comparisons test.

3. Results and Discussion

3.1. Material Synthesis and Microgel Fabrication

A supramolecular hydrogel was first fabricated using guest-host interactions of modified HA. Separately, HA was modified with adamantane (guest, ~20% modification) to form AdHA and ß-cyclodextrin (host, ~20% modification) to form CDHA (Figure 1A). AdHA and CDHA components, upon mixing, have been previously shown to assemble due to hydrophobic interactions to form supramolecular, host-guest complexes that disassemble upon the application of shear but also rapidly re-assemble to form a stable hydrogel after injection (Figure 1B,C)[48]. The injectable properties of this hydrogel have been previously explored[47] as injectable hydrogels are particularly attractive for clinical translation because they can improve the retention of delivered therapeutics and be delivered using minimally invasive approaches like catheters[35]. Variations of this bulk guest-host hydrogel have been previously investigated in our lab to deliver cells[20], exosomes[49], small molecules[23], growth factors[19,21], and RNAs[38,50].

To form microgels, HA was modified with norbornene groups (~30% modification) to form NorHA (Figure 1A). Norbornenes react to form covalent bonds via thiol-ene reactions with thiols in the presence of UV light and a photoinitiator (Figure 1D)[51], which can be used to form microgels (Figure 1E). There are numerous techniques that can be used to fabricate covalently-crosslinked microgels, primarily through water-in-oil emulsion techniques[52,53]. Here, microgels were fabricated using a recently developed microfluidic device[40] to generate particles that were crosslinked with UV light as they flowed out of the device and into a collection vial (Figure 2A-C). Microgels were spherical and generally uniform in size with a diameter of 59 ± 7 μm (Figure 2D,E).

To encapsulate a therapeutic, such as IL-10, the therapeutic was simply added to the aqueous phase during microgel processing. Thiolated heparin, which has a high density of negative charge, was also incorporated into the microgels to sequester positively-charged IL-10 prior to release. When we compared the encapsulation efficiency, or the ratio of the amount of IL-10 detected to the amount of IL-10 expected, we found that the encapsulation efficiency of microgels formulated with HepSH (17.3% ± 7.2) was significantly higher than that of microgels formulated without HepSH (2.6% ± 0.3) (Supplementary Figure 2A; mean ± SD). The remaining IL-10 could have been lost during the microgel formation process or during ELISA analysis. The zeta potential of microgel precursor solutions of NorHA with HepSH (−21.5 ± 1.2 mV) was significantly more negative than the zeta potential of solutions of NorHA alone (−10.0 ± 1.6 mV) (Supplementary Figure 2B; mean ± SD). Thus, HepSH was deemed important for IL-10 encapsulation and was used in all subsequent studies.

Microgels crosslinked with either a stable (DTT) or hydrolytically degradable (PETMA) crosslinker were fabricated and assessed for degradation and IL-10 release over 2 weeks (Figure 3A). The degradable microgels were fully degraded after 2 weeks, while stable microgels were still largely intact (Figure 3B). Similar trends were observed for IL-10 release (Figure 3C), with IL-10 completely released within 2 weeks from the degradable microgels, whereas stable microgels still retained much of their IL-10 content. Thus, we observed that microgel stability and the rate of therapeutic delivery can be tailored by

changing the stability of the thiol crosslinker within the microgels. For more complex growth factor cocktails and delivery profiles, microgels of varying stability could be combined. For IL-10 delivery in our study, we desired the steady release of IL-10 from microgels over a few weeks to match doses from previous IL-10 delivery studies and to correspond to detected expression patterns of IL-10 in various animal MI models; thus, for animal studies we selected degradable microgels [54–56].

3.2. Composite Fabrication and Characterization

To combine the benefits of injectability from the bulk guest-host hydrogel and the controlled release of microgels, they were combined to fabricate composites (Figure 4A). With this approach, microgels can be designed with differing levels of stability and added at different loading amounts and even with mixed compositions to control release, independent of the design of the bulk guest-host hydrogel. Others have previously explored the use of nano-scale particles (<1 μm) for drug delivery from composites[24,57]; here, we use micro-scale particles and investigate the material properties of these composite hydrogels to learn more about the network interactions between the bulk guest-host hydrogel and covalently-crosslinked microgels.

Microgels were combined with the bulk guest-host hydrogel to form a composite hydrogel at low (6.7 mg microgels/mL bulk hydrogel) or high (13.3 mg microgels/mL bulk hydrogel) concentrations and characterized through confocal microscopy to visualize fluorescently labeled microgels (Figure 4B). The volume fraction of microgels within the bulk hydrogel for the low concentration was 0.08 ± 0.02 and for the high concentration was significantly higher at 0.29 ± 0.05 (Figure 4C, mean ± SD). This illustrates our ability to alter the loading of microgels and encapsulated therapeutics. Although there is no specific interaction intended between the bulk guest-host hydrogel and the covalently-crosslinked microgels, entanglement of the bulk hydrogel within the covalent network during encapsulation or non-specific interactions between the β-cyclodextrin and norbornene groups are possible.

The material properties of the bulk guest-host hydrogel, the low microgel composite hydrogel, and the high microgel composite hydrogel were evaluated using oscillatory shear rheometry. All groups behaved as hydrogels (G’ > G”) (Figure 5A) that were viscoelastic, as indicated by changes in the moduli with variations in frequency (Figure 5B). The high microgel composite hydrogel had the lowest crossover frequency (~0.1 Hz) and therefore the longest relaxation time, indicating that this hydrogel flows less than the low microgel composite hydrogel or the bulk guest-host hydrogel, which had similar crossover frequencies (~2 Hz for bulk hydrogel, ~ 1 Hz for the low microgel composite hydrogel). The granular nature of the composite hydrogels and the covalent-crosslinking of the microgels likely contributes to the longer relaxation times.

All groups behaved rheologically as shear-thinning injectable materials. The strain sweeps indicated material yielding, or a decline in storage and loss moduli at particular strains (Figure 5C). Interestingly, the composites yielded at lower strains than the bulk hydrogel, likely due to failure at interfaces between the supramolecular hydrogel and covalently-crosslinked microgels. Continuous flow experiments also showed a decrease in viscosity for all groups with increasing shear rate, indicative of shear-thinning (Figure 5D). Both

composite hydrogels showed evidence of shear banding, a phenomenon in which portions of the hydrogel undergo shear and are liquidized while other portions of the hydrogel remain solid, allowing the same shear stress to be achieved at 2 or more shear rates[58] (Figure 5E). At high strains, the storage and loss moduli for all groups decreased, but then recovered upon the cessation of strain, indicative of self-healing (Figure 5F).

Hydrogels with lower storage and loss moduli (at high strains relevant for injection), lower yield strain, and lower viscosity are typically easier to inject than hydrogels with higher storage and loss moduli, higher yield strain, and higher viscosity. Based on these criteria and observations during handling, the composite hydrogels are easier to inject than then the bulk guest-host hydrogel. The granular nature of these composite hydrogels potentially makes them more prone to shear banding[59,60], which also improves injectability. To balance injectability and therapeutic dosage, the high microgel composite hydrogels were used in animal studies to assess them for use in the delivery of IL-10.

Additionally, we investigated the release of IL-10 from these high microgel composite hydrogels compared to microgels alone (Supplementary Figure 3). After 2 weeks, only ~15% of the encapsulated IL-10 was released in the composite hydrogels, whereas the microgels alone were fully degraded at the end of 2 weeks with 100% of the encapsulated IL-10 released. This suggests that the bulk gel can further modulate IL-10 release, and can be engineered to further tune the release profile of encapsulated therapeutics. Encapsulation of microgels within the bulk gel also eliminated burst release effects. However, *in vivo* and *in vitro* release kinetics may differ due to the contractile nature of the heart. For example, in previous studies we have observed that the bulk hydrogel is 90% eroded at the end of 1 week *in vivo*, but persists for over 3 weeks *in vitro*[38]. Ultimately, it is necessary to entrap microgels within the bulk hydrogel to improve localization of the therapy to the injection site and prevent the dispersion of microgels if delivered alone[57].

3.3. Rat MI Model

Following MI, PBS, composites without IL-10, or composites with IL-10 were injected into the border zone region of the infarct (Figure 6A,B). IL-10 is produced by activated T cells and monocytes after MI[41] and reduces inflammation by both mediating the transition of macrophages from a pro-inflammatory M1 phenotype to an anti-inflammatory M2 phenotype[61,62] and by downregulating the production of inflammatory cytokines such as IL-1α, IL-1β, TNF-α, IL-6, IL-8, and IL-12 by monocytes and macrophages via the STAT3 pathway[41,42,63]. To better understand the influence of exogenous IL-10 delivery on treating MI, the immune response was evaluated with CD68 staining for macrophages after 1 week and remodeling, cardiac function, and vasculature outcomes were assessed after 4 weeks (Figure 6C).

Representative images of immunohistochemistry for CD68 after 1 week are shown (Figure 7A-F). CD68 is a marker commonly expressed by activated or inflammatory macrophages, which play a critical role in the acute inflammatory response after MI, but excess activity can lead to increased tissue damage[41,64]. CD68 staining showed the presence of macrophages in the border zone region of the infarct for all treatment groups. When quantified, $CD68^+$ area fraction showed that delivery of composites with IL-10 significantly

decreased the presence of CD68+ macrophages when compared to saline delivery, which indicates that IL-10 delivery can mitigate inflammation near the injection site (Figure 7G). There was a non-statistically significant decrease in $CD68^+$ staining with the composite releasing IL-10 when compared to the composite without IL-10.

After 4 weeks, Masson's trichrome staining was used to visualize scar tissue after the delivery of saline, composites without IL-10, or composites with IL-10 (Figure 8A-C). Notably, HA composite hydrogel/microgel structures were still visible (Figure 8D-E), which was confirmed to be glycosaminoglycans (i.e., HA) through Alcian blue staining (Supplementary Figure 4A-D). Quantification of scar fraction showed no difference among groups (Supplementary Figure 4E); however, there was increased scar thickness with the delivery of composites, and this improvement was significant for the delivery of composites with IL-10 compared to saline delivery (Figure 8F).

Scar thickening in the presence of the composite hydrogels is likely due to them acting as bulking agents. Previous work by our group has shown that the bulk guest-host hydrogel by itself is not intact and almost completely eroded after 4 weeks[38,65]; however, the microgels likely remain longer in the tissue. Microparticles have been introduced via biomaterials into infarcted tissue previously and have improved functional outcomes through a bulking response, likely through altering the inflammatory response[66,67]. In addition to a response of the microgels alone, IL-10 has been found to have inhibitory effects on matrix metalloproteinases and increase production of tissue inhibitor matrix metalloproteinases by human macrophages in cell culture models, indicating the role of IL-10 in limiting the adverse remodeling of native tissues[68]. Combined, the effect of the composite hydrogel as a bulking agent with the therapeutic delivery of anti-inflammatory IL-10 showed significant improvements in scar thickness over the saline control, which may correspond to improvements in cardiac function.

After 4 weeks, pressure-volume catheterization was used to assess cardiac function by measuring hemodynamics after the delivery of saline, composites without IL-10, or composites with IL-10 (Figure 9A-D). The delivery of composites without IL-10 showed significant improvements in ejection fraction and dP/dt_{max}, a measure of cardiac contractility, compared to saline delivery. The delivery of composites with IL-10 showed significant improvements in ejection fraction, cardiac output, dP/dt_{max}, and preload recruitable stroke work (PRSW; another index of myocardial contractility) compared to saline and in PRSW when compared to the composites without IL-10. For ejection fraction, cardiac output, dP/dt_{max}, and PRSW, the delivery of composites with or without IL-10 also improved the value of these outcomes to healthy baseline levels.

The improvement of cardiac function with the delivery of composites without IL-10 indicates that the material itself has a positive effect, likely due to its ability to act as a bulking agent and thicken the left ventricular wall. According to the Laplace's law, wall thickness is inversely proportional to wall stress, so thickening of the left ventricular wall can decrease wall stress and prevent further ventricular dilation that can lead to poor cardiac function[34,35]. The additional improvements in cardiac function exhibited by the delivery of composites with IL-10 indicate that the anti-inflammatory effect of IL-10 may help to

mitigate the tissue damage that can be caused by excessive inflammation and initiate the healing process[42,69].

After 4 weeks, immunohistochemistry was used to assess the density and size of vascular structures after the delivery of saline, composites without IL-10, or composites with IL-10 and representative images are shown (Figure 10A-C). Von Willebrand factor, or vWF, is a glycoprotein produced by endothelial cells and is present in the lumen of vascular structures of all sizes, from capillaries to arterioles[70,71], whereas alpha-smooth muscle actin (α-SMA) is expressed by smooth muscle cells and is only present in more mature vasculature[71]. Both vWF^+ and $vWF^+\alpha\text{-}SMA^+$ vascular structures contribute to enhancing perfusion in the border zone region after MI. Quantification of vWF^+ area showed that the delivery of composites without or with IL-10 significantly increased vWF^+ area compared to the delivery of saline (Figure 10D). Quantification of $vWF^+\alpha\text{-}SMA^+$ structure sizes showed that the delivery of composites without or with IL-10 increased structure size but only the delivery of composites with IL-10 significantly increased structure size compared to the delivery of saline (Figure 10E).

These results indicate that the composite hydrogel alone has a positive effect on vascular density, and that the effects of the composite hydrogel and IL-10 can combine to have an even greater result. Larger vessel diameters are often correlated with more mature vessels that are more constructive for improved remodeling and functional outcomes, which makes the influence of IL-10 delivery on vessel size important[72]. Systemic IL-10 has also been shown to increase the number of vascular structures after delivery of endothelial progenitor cells (EPCs) in MI compared to the delivery of EPCs without IL-10, further emphasizing the role of IL-10 in vascularization[73]. HA has also been shown to improve vascularization, largely due to the role of HA in cell migration and proliferation[74–76].

4. Conclusions

An injectable bulk guest-host hydrogel was combined with covalently-crosslinked microgels to create a composite hydrogel/microgel for therapeutic delivery, combining the beneficial properties of both systems. By encapsulating therapeutics within microgels, the release of therapeutics from this composite hydrogel was decoupled from the degradation of the bulk hydrogel. The composite hydrogel was shear-thinning, self-healing, and injectable. As a model therapeutic, IL-10 was delivered using this composite hydrogel after MI. The delivery of composites with IL-10 significantly decreased the presence of macrophages after 1 week and increased scar thickness, improved cardiac function, and enhanced vascular density after 4 weeks compared to saline delivery. The composite hydrogel/microgel system described here could be tuned for the delivery of multiple therapeutics with complex release profiles for broad applications.

Supplementary Material

Refer to Web version on PubMed Central for supplementary material.

Acknowledgements

The authors would like to acknowledge Mi Y. Kwon for her help with the zeta potential measurements, Jonathan S. Gordon for his contributions to the animal studies, and H.H. Jeong, D. Issadore, and D. Lee for development and assistance with the microfluidic device. This work was made possible by financial support from a predoctoral fellowship from the American Heart Association (to MHC), a National Science Foundation Graduate Research Fellowship (to JEM), and the National Institutes of Health (T32AR007132, R01HL135090, R01HL063954).

References

[1]. Hoffman AS, Adv. Drug Deliv. Rev 2012, 64, 18.

[2]. Webber MJ, Appel EA, Meijer EW, Langer R, Nat. Mater 2015, 15, 13.

[3]. Guvendiren M, Lu HD, Burdick JA, Soft Matter 2012, 8, 260.

[4]. Dong R, Pang Y, Su Y, Zhu X, Biomater. Sci 2015, 3, 937. [PubMed: 26221932]

[5]. Hartgerink JD, Science (80-.). 2001, 294, 1684.

[6]. Gelain F, Horii A, Zhang S, Macromol. Biosci 2007, 7, 544. [PubMed: 17477441]

[7]. Zhou M, Smith AM, Das AK, Hodson NW, Collins RF, Ulijn RV, Gough JE, Biomaterials 2009, 30, 2523. [PubMed: 19201459]

[8]. Cui H, Webber MJ, Stupp SI, Pept. Sci 2010, 94, 1.

[9]. Appel E. a., Biedermann F, Rauwald U, Jones ST, Zayed JM, Scherman O. a., J. Am. Chem. Soc 2010, 14251. [PubMed: 20845973]

[10]. Appel EA, Del Barrio J, Loh XJ, Scherman OA, Chem. Soc. Rev 2012, 41, 6195. [PubMed: 22890548]

[11]. Rodell CB, Kaminski AL, Burdick JA, Biomacromolecules 2013, 1. [PubMed: 23157442]

[12]. Lu HD, Charati MB, Kim IL, Burdick JA, Biomaterials 2012, 33, 2145. [PubMed: 22177842]

[13]. Gao Y, Shi J, Yuan D, Xu B, Nat. Commun 2012, 3, 1033. [PubMed: 22929790]

[14]. Hsu SM, Wu FY, Cheng H, Huang YT, Hsieh YR, Tseng DTH, Yeh MY, Hung SC, Lin HC, Adv. Healthc. Mater 2016, 5, 2406. [PubMed: 27390271]

[15]. Dankers PYW, Meijer EW, Bull. Chem. Soc. Jpn 2007, 80, 2047.

[16]. Dankers PYW, Harmsen MC, Brouwer LA, Van Luyn MJA, Meijer EW, Nat. Mater 2005, 4, 568. [PubMed: 15965478]

[17]. Parisi-Amon A, Mulyasasmita W, Chung C, Heilshorn SC, Adv. Healthc. Mater 2013, 2, 428. [PubMed: 23184882]

[18]. Webber MJ, Tongers J, Renault M, Roncalli JG, Losordo DW, Stupp SI, Acta Biomater 2009, 6 VN-re, 3. [PubMed: 19635599]

[19]. Rodell CB, Rai R, Faubel S, Burdick JA, Soranno DE, Control J. Release 2015, 206, 131.

[20]. Gaffey AC, Chen MH, Venkataraman CM, Trubelja A, Rodell CB, Dinh PV, Hung G, MacArthur JW, Soopan RV, Burdick JA, Atluri P., J. Thorac. Cardiovasc. Surg 2015, 19104, DOI 10.1016/j.jtcvs.2015.07.035.

[21]. Soranno DE, Rodell CB, Altmann C, Duplantis J, Andres-Hernando A, Burdick JA, Faubel S, Am. J. Physiol. Physiol 2016, 311, F362.

[22]. Rodell CB, Wade RJ, Purcell BP, Dusaj NN, Burdick JA, ACS Biomater. Sci. Eng 2015, 1, 277.

[23]. Mealy JE, Rodell CB, Burdick JA, J. Mater. Chem. B 2015, 3, 8010. [PubMed: 26693019]

[24]. Appel EA, Tibbitt MW, Webber MJ, Mattix BA, Veiseh O, Langer R, Nat. Commun 2015, 6, 1.

[25]. Tous E, Purcell B, Ifkovits JL, Burdick JA, J. Cardiovasc. Transl. Res 2011, 4, 528. [PubMed: 21710332]

[26]. Hasan A, Khattab A, Islam MA, Hweij KA, Zeitouny J, Waters R, Sayegh M, Hossain MM, Paul A, Adv. Sci 2015, 2, 1.

[27]. Benjamin EJ, Blaha MJ, Chiuve SE, Cushman M, Das SR, Deo R, de Ferranti SD, Floyd J, Fornage M, Gillespie C, Isasi CR, Jiménez MC, Jordan LC, Judd SE, Lackland D, Lichtman JH, Lisabeth L, Liu S, Longenecker CT, Mackey RH, Matsushita K, Mozaffarian D, Mussolino ME, Nasir K, Neumar RW, Palaniappan L, Pandey DK, Thiagarajan RR, Reeves MJ, Ritchey M, Rodriguez CJ, Roth GA, Rosamond WD, Sasson C, Towfighi A, Tsao CW, Turner MB, Virani

SS, Voeks JH, Willey JZ, Wilkins JT, HYWu J., Alger HM, Wong SS, Muntner P, Heart Disease and Stroke Statistics—2017 Update: A Report From the American Heart Association, 2017.

[28]. Torabi A, Cleland JG, Rigby AS, Sherwi N, J. Geriatr. Cardiol 2014, 11, 1. [PubMed: 24748875]

[29]. Mozaffarian D, Benjamin EJ, Go AS, Arnett DK, Blaha MJ, Cushman M, Das SR, de Ferranti S, Després J-P, Fullerton HJ, Howard VJ, Huffman MD, Isasi CR, Jiménez MC, Judd SE, Kissela BM, Lichtman JH, Lisabeth LD, Liu S, Mackey RH, Magid DJ, McGuire DK, Mohler ER, III, Moy CS, Munter P, Mussolino ME, Nasir K, Neumar RW, Nichol G, Palaniappan L, Pandey DK, Reeves MJ, Rodriguez CJ, Rosamond W, Sorlie PD, Stein J, Towfighi A, Turan TN, Virani SS, Woo D, Yeh RW, Turner MB, Heart Disease and Stroke Statistics—2016 Update, 2015.

[30]. Christman KL, Lee RJ, J. Am. Coll. Cardiol 2006, 48, 907. [PubMed: 16949479]

[31]. Burdick JA, Mauck RL, Gorman JH, Gorman RC, Sci. Transl. Med 2013, 5, 1.

[32]. Rao SV, Zeymer U, Douglas PS, Al-Khalidi H, White JA, Liu J, Levy H, Guetta V, Gibson CM, Tanguay JF, Vermeersch P, Roncalli J, Kasprzak JD, Henry TD, Frey N, Kracoff O, Traverse JH, Chew DP, Lopez-Sendon J, Heyrman R, Krucoff MW, J. Am. Coll. Cardiol 2016, 68, 715. [PubMed: 27515331]

[33]. Mann DL, Lee RJ, Coats AJS, Neagoe G, Dragomir D, Pusineri E, Piredda M, Bettari L, Kirwan B, Dowling R, Volterrani M, Solomon SD, Sabbah HN, Hinson A, Anker SD, Eur. J. Heart Fail 2015, 18, 314. [PubMed: 26555602]

[34]. Yin FCP, Circ. Res 1981, 49, 829. [PubMed: 7023741]

[35]. Rodell CB, Lee ME, Wang H, Takebayashi S, Takayama T, Kawamura T, Arkles JS, Dusaj NN, Dorsey SM, Witschey WRT, Pilla JJ, Gorman JH, III, Wenk JF, Burdick JA, Gorman RC, Circ Cardiovasc Interv 2016, 9, DOI 10.1016/j.chembiol.2009.02.014.A.

[36]. Chen WCW, Lee BG, Park DW, Kim K, Chu H, Kim K, Huard J, Wang Y, Biomaterials 2015, 72, 138. [PubMed: 26370927]

[37]. Johnson NR, Kruger M, Goetsch KP, Zilla P, Bezuidenhout D, Wang Y, Davies NH, ACS Biomater. Sci. Eng 2015, 1, 753.

[38]. Wang LL, Liu Y, Chung JJ, Wang T, Gaffey AC, Lu M, Cavanaugh CA, Zhou S, Kanade R, Atluri P, Morrisey EE, Burdick JA, Nat. Biomed. Eng 2017, 1, 983. [PubMed: 29354322]

[39]. Singelyn JM, Sundaramurthy P, Johnson TD, Schup-Magoffin PJ, Hu DP, Faulk DM, Wang J, Mayle KM, Bartels K, Salvatore M, Kinsey AM, DeMaria AN, Dib N, Christman KL, J Am Coll Cardiol 2012, 59, 751. [PubMed: 22340268]

[40]. Jeong H-H, Yelleswarapu VR, Yadavali S, Issadore D, Lee D, Lab Chip 2015, 15, 4387. [PubMed: 26428950]

[41]. Frangogiannis N, Cardiovasc. Res 2002, 53, 31. [PubMed: 11744011]

[42]. Frangogiannis NG, Circ. Res 2012, 110, 159. [PubMed: 22223212]

[43]. Vega SL, Kwon MY, Song KH, Wang C, Mauck RL, Han L, Burdick JA, Nat. Commun 2018, 9, 614. [PubMed: 29426836]

[44]. Tae G, Kim YJ, Il Choi W, Kim M, Stayton PS, Hoffman AS, Biomacromolecules 2007, 8, 1979. [PubMed: 17511500]

[45]. Jha AK, Tharp KM, Ye J, Santiago-Ortiz JL, Jackson WM, Stahl A, Schaffer DV, Yeghiazarians Y, Healy KE, Biomaterials 2015, 47, 1. [PubMed: 25682155]

[46]. Mealy JE, Chung JJ, Jeong HH, Issadore D, Lee D, Atluri P, Burdick JA, Adv. Mater 2018, 30, 1.

[47]. Chen MH, Wang LL, Chung JJ, Kim YH, Atluri P, Burdick JA, ACS Biomater. Sci. Eng 2017, 3, 3146. [PubMed: 29250593]

[48]. Rodell CB, Kaminski AL, Burdick JA, Biomacromolecules 2013, 14, 4125. [PubMed: 24070551]

[49]. Chen CW, Wang LL, Zaman S, Gordon J, Arisi MF, Venkataraman CM, Chung JJ, Hung G, Gaffey AC, Spruce LA, Fazelinia H, Gorman RC, Seeholzer SH, Burdick JA, Atluri P, Cardiovascular Research 2018, 114, 1029. [PubMed: 29566124]

[50]. Wang LL, Sloand JN, Gaffey AC, Venkataraman CM, Wang Z, Trubelja A, Hammer DA, Atluri P, Burdick JA, Biomacromolecules 2017, 18, 77. [PubMed: 27997133]

[51]. Gramlich WM, Kim IL, Burdick JA, Biomaterials 2013, 34, 9803. [PubMed: 24060422]

[52]. Kesselman LRB, Shinwary S, Selvaganapathy PR, Hoare T, Small 2012, 8, 1092. [PubMed: 22354786]

[53]. Liu AL, García AJ, Ann. Biomed. Eng 2016, 44, 1946. [PubMed: 27160672]

[54]. Krishnamurthy P, Rajasingh J, Lambers E, Qin G, Losordo DW, Kishore R, Circ. Res 2009, 104, 9. [PubMed: 19118282]

[55]. Dewald O, Ren G, Duerr GD, Zoerlein M, Klemm C, Gersch C, Tincey S, Michael LH, Entman ML, Frangogiannis NG, Am. J. Pathol 2004, 164, 665. [PubMed: 14742270]

[56]. Frangogiannis NG, Mendoza LH, Lindsey ML, Ballantyne CM, Michael LH, Smith CW, Entman ML, Immunol J. 2000, 165, 2798.

[57]. Sivakumaran D, Maitland D, Hoare T, Biomacromolecules 2011, 12, 4112. [PubMed: 22007750]

[58]. Chen DTN, Wen Q, Janmey PA, Crocker JC, Yodh AG, *Annu. Rev.* Condens. Matter Phys 2010, 1, 301.

[59]. Losert W, Bocquet L, Lubensky TC, Gollub JP, Phys. Rev. Lett 2000, 85, 1428. [PubMed: 10970521]

[60]. Fardin MA, Ober TJ, Gay C, Grégoire G, McKinley GH, Lerouge S, Soft Matter 2012, 8, 910.

[61]. Mantovani A, Biswas SK, Galdiero MR, Sica A, Locati M, J. Pathol 2013, 229, 176. [PubMed: 23096265]

[62]. Browne S, Pandit A, Front. Bioeng. Biotechnol 2015, 3, DOI 10.3389/fbioe.2015.00067.

[63]. de W. Malefyt R, Abrams J, Bennett B, Figdor CG, de Vries JE, J. Exp. Med 1991, 174, 1209. [PubMed: 1940799]

[64]. Chávez-Galán L, Olleros ML, Vesin D, Garcia I, Front. Immunol 2015, 6, 1. [PubMed: 25657648]

[65]. Rodell CB, MacArthur JW, Dorsey SM, Wade RJ, Wang LL, Woo YJ, Burdick JA, Adv. Funct. Mater 2015, 25, 636. [PubMed: 26526097]

[66]. Tous E, Weber HM, Lee MH, Koomalsingh KJ, Shuto T, Kondo N, Gorman JH, Lee D, Gorman RC, Burdick JA, Acta Biomater 2012, 8, 3218. [PubMed: 22659176]

[67]. McGarvey JR, Pettaway S, Shuman JA, Novack CP, Zellars KN, Freels PD, Echols RL, Burdick JA, Gorman JH, Gorman RC, Spinale FG, J. Pharmacol. Exp. Ther 2014, 350, 701. [PubMed: 25022514]

[68]. Lacraz S, Nicod LP, Chicheportiche R, Welgus HG, Dayer J-M, J. Clin. Invest 1995, 96, 2304. [PubMed: 7593617]

[69]. Frangogiannis NG, Nat. Rev. Cardiol 2014, 11, 255. [PubMed: 24663091]

[70]. Hassan MI, Saxena A, Ahmad F, Blood Coagul. Fibrinolysis 2012, 23, 11. [PubMed: 22089939]

[71]. Carmeliet P, Nat. Med 2000, 6, 389. [PubMed: 10742145]

[72]. Conway EM, Collen D, Carmeliet P, Cardiovasc. Res 2001, 49, 507. [PubMed: 11166264]

[73]. Krishnamurthy P, Thal M, Verma S, Hoxha E, Lambers E, Ramirez V, Qin G, Losordo D, Kishore R, Circ. Res 2011, 109, 1280. [PubMed: 21959218]

[74]. Necas J, Bartosikova L, Brauner P, Kolar J, Vet. Med. (Praha). 2008, 397.

[75]. Pardue EL, Ibrahim S, Ramamurthi A, Organogenesis 2008, 4, 203. [PubMed: 19337400]

[76]. Park D, Kim Y, Kim H, Kim K, Lee YS, Choe J, Hahn JH, Lee H, Jeon J, Choi C, Kim Y-M,Jeoung D, Mol. Cells 2012, 33, 563. [PubMed: 22610405]

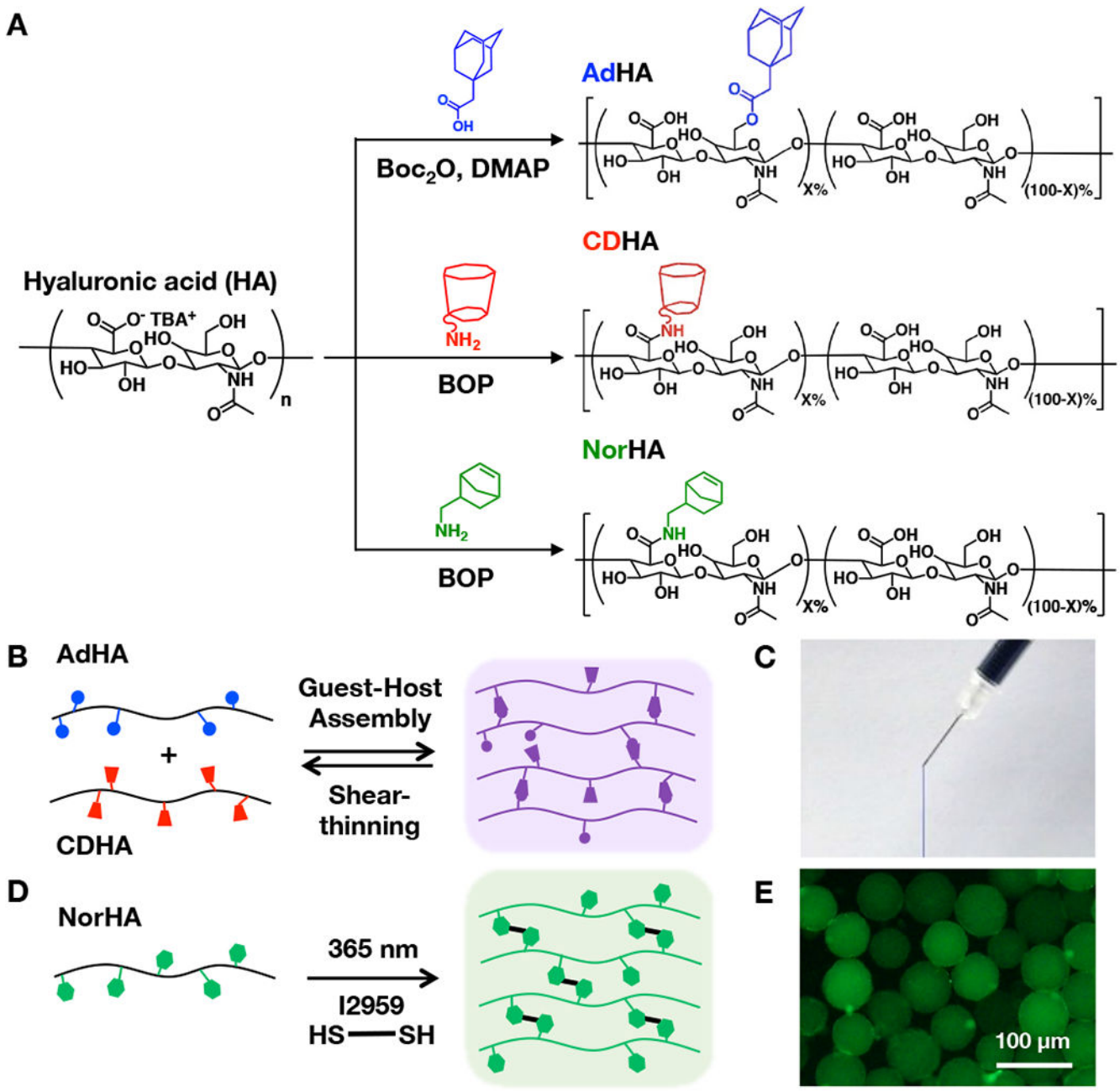

Figure 1.

A) Reaction schematics for the synthesis of adamantane-modified HA (AdHA, ~20% modification), cyclodextrin-modified HA (CDHA, ~20% modification), and norbornene-modified HA (NorHA, ~30% modification). B) AdHA and CDHA assemble into a hydrogel through guest-host complexes upon mixing that disassemble upon the application of shear, resulting in an C) injectable guest-host hydrogel (dyed blue) that can be extruded from a syringe and rapidly self-heals after injection. D) NorHA crosslinks through a thiol-ene reaction in the presence of a di-thiol crosslinker, photoinitiator, and UV light and can be

processed into E) covalently-crosslinked NorHA microgels (visualized with encapsulated FITC-dextran).

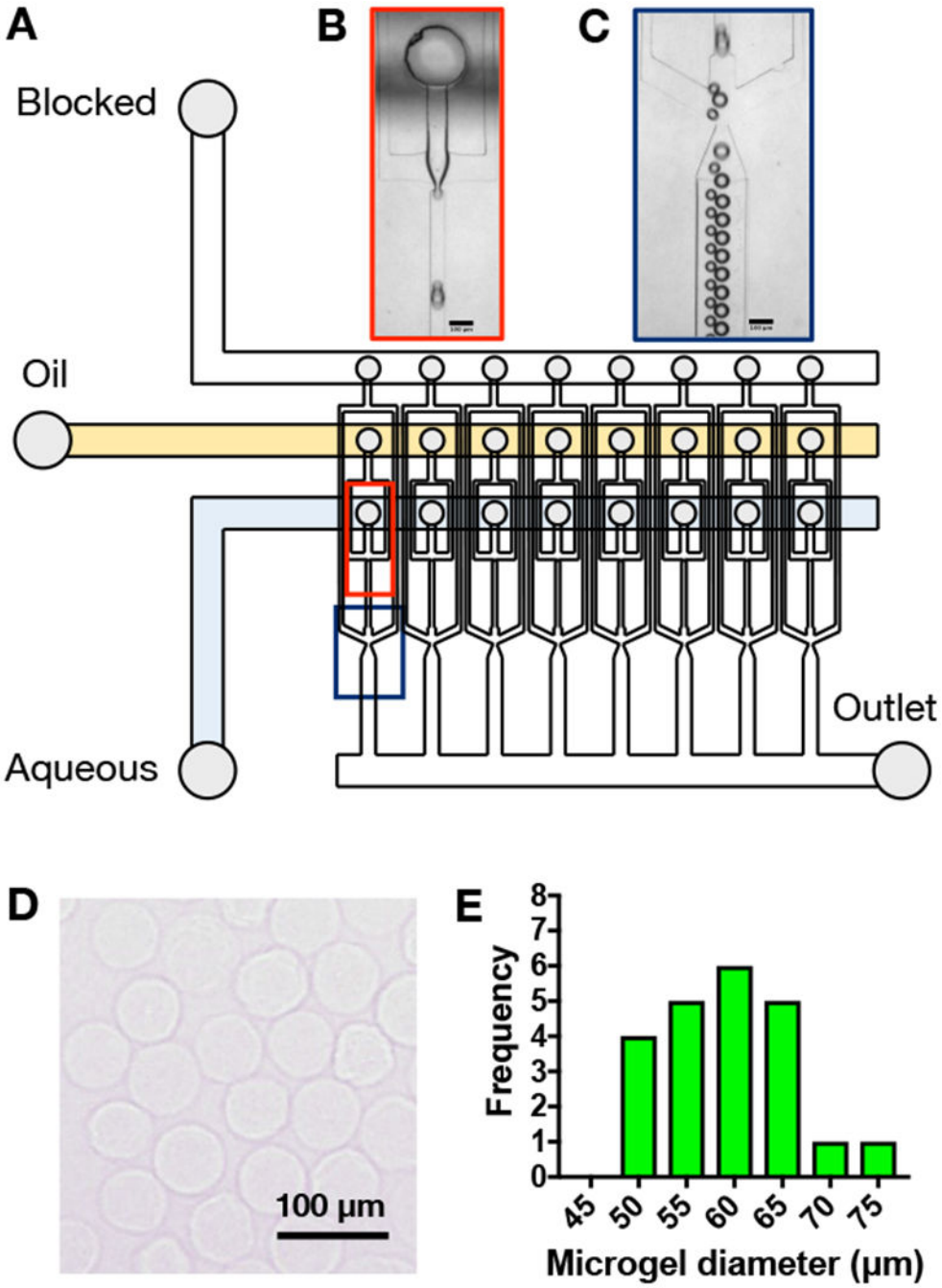

Figure 2.

A) Schematic of high-throughput microfluidic device for water-in-oil droplet formation and screenshots (scale bars = 100 μm) of droplets B) being formed and C) flowing through the device. After crosslinking with UV light, microgels were washed from the oil, dehydrated for storage, and then rehydrated to form relatively uniform spherical microgels as D) visualized with light microscopy and E) quantified as a histogram with an average microgel diameter of 59 ± 7 μm (mean ± SD).

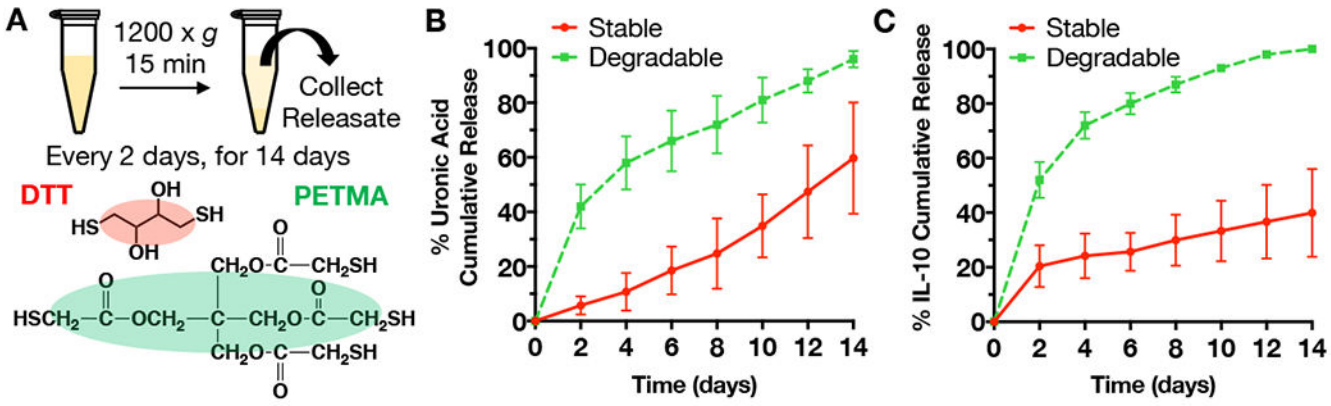

Figure 3.

A) Schematic for microgel degradation and release studies. Microgels were fabricated with either stable (DTT as crosslinker) or hydrolytically degradable (PETMA as crosslinker) crosslinks, washed, and incubated in release buffer for up to 14 days. At each sample point, microgels were centrifuged at 1200 × *g* for 15 minutes and then releasate was collected for analysis of HA degradation products and IL-10 release. After 14 days, the microgels were fully degraded in hyaluronidase for analysis of any remaining uronic acid or IL-10. B) Uronic acid and C) IL-10 cumulative release over 14 days (mean ± SD).

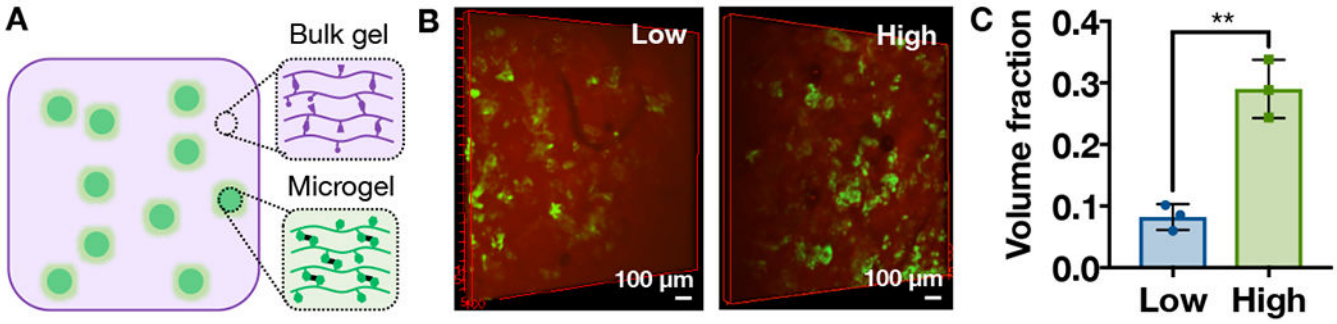

Figure 4.

A) Schematic of supramolecular hydrogel/microgel composite, consisting of bulk guest-host hydrogel (purple) with encapsulated microgels (green). B) 3D projections of microgels (green) in bulk guest-host hydrogels (red) at low (left, 6.7 mg/mL bulk hydrogel) or high (right, 13.3 mg/mL bulk hydrogel) concentrations. C) Volume fraction of microgels in the bulk guest-host hydrogel at low and high concentrations (mean ± SD, n=3, *p<0.05, **p<0.01).

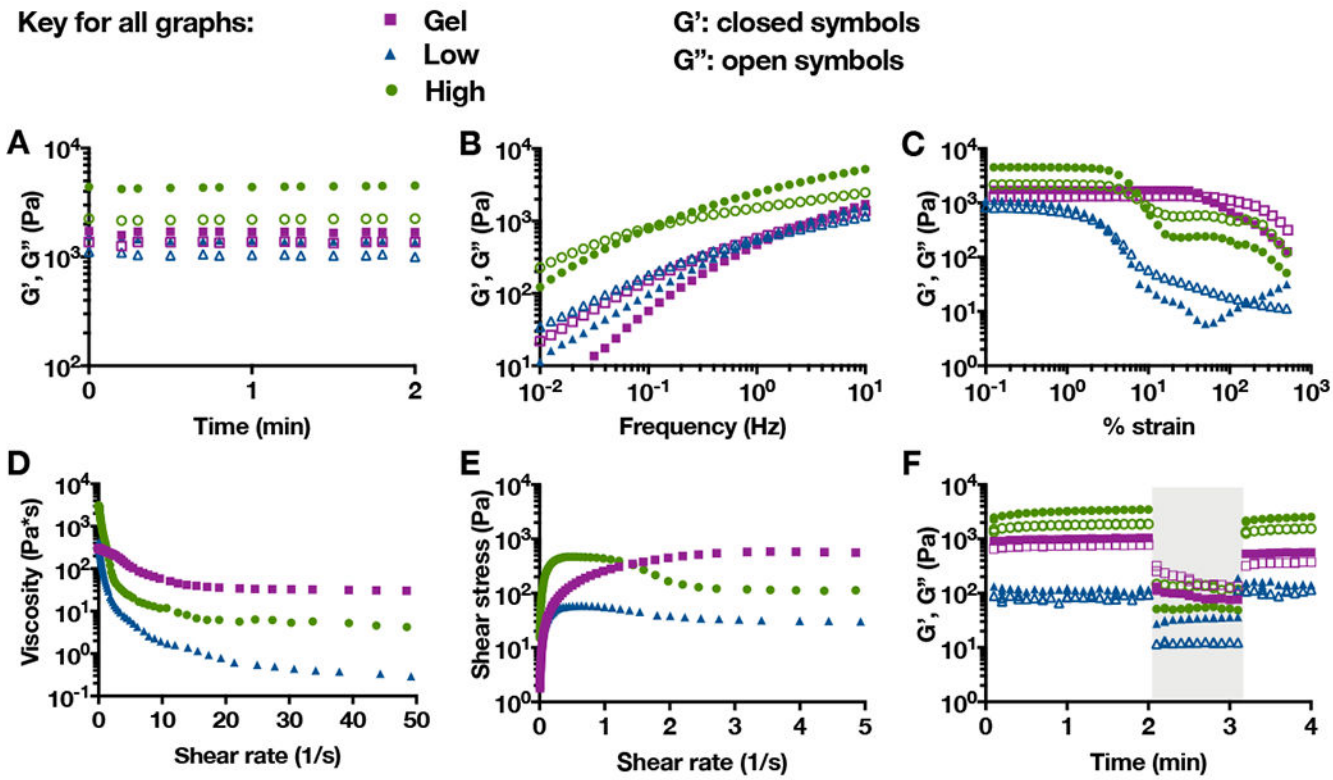

Figure 5.

Bulk guest-host hydrogels alone (Gel) or as microgel composites at a low (6.7 mg/mL bulk hydrogel) or high (13.3 mg/mL bulk hydrogel) microgel concentration characterized using oscillatory shear rheometry, including: storage (G', closed symbols) and loss (G'', open symbols) moduli A) over time at 0.2% strain and 10 Hz, B) across a range of frequencies at 0.2% strain, C) across a range of % strains at 10 Hz, D) viscosity with increasing shear rate, E) shear stress with increasing shear rate, and F) cyclic strains over time (low = 0.2% strain at 10 Hz, high (shaded) = 500% strain at 10 Hz).

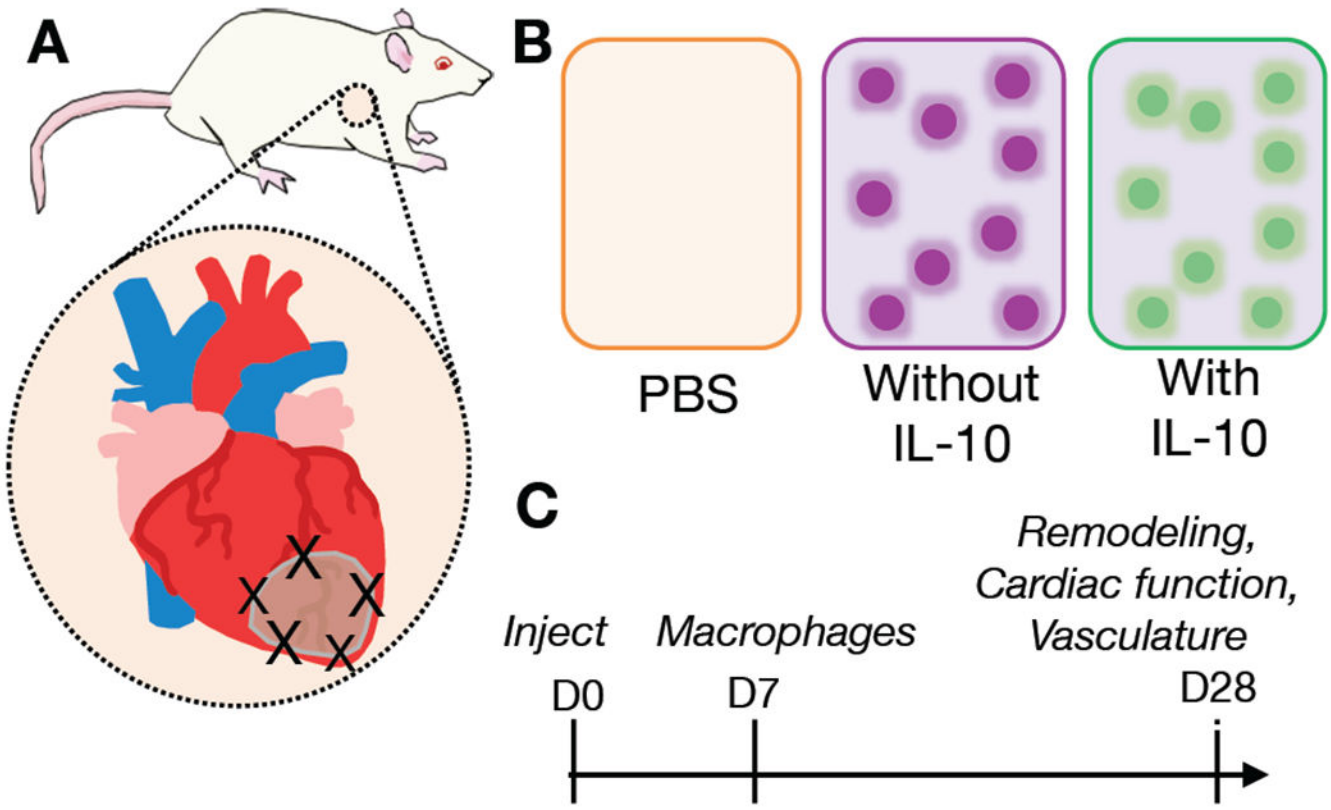

Figure 6.

Schematic of the analysis of composite hydrogels in a rat MI model, including A) injection sites in border zone of MI after LAD ligation, B) treatment groups of saline control (PBS), composites without IL-10, and composites with IL-10, C) experimental design timeline showing injection at day 0 and outcome measures after 7 and 28 days.

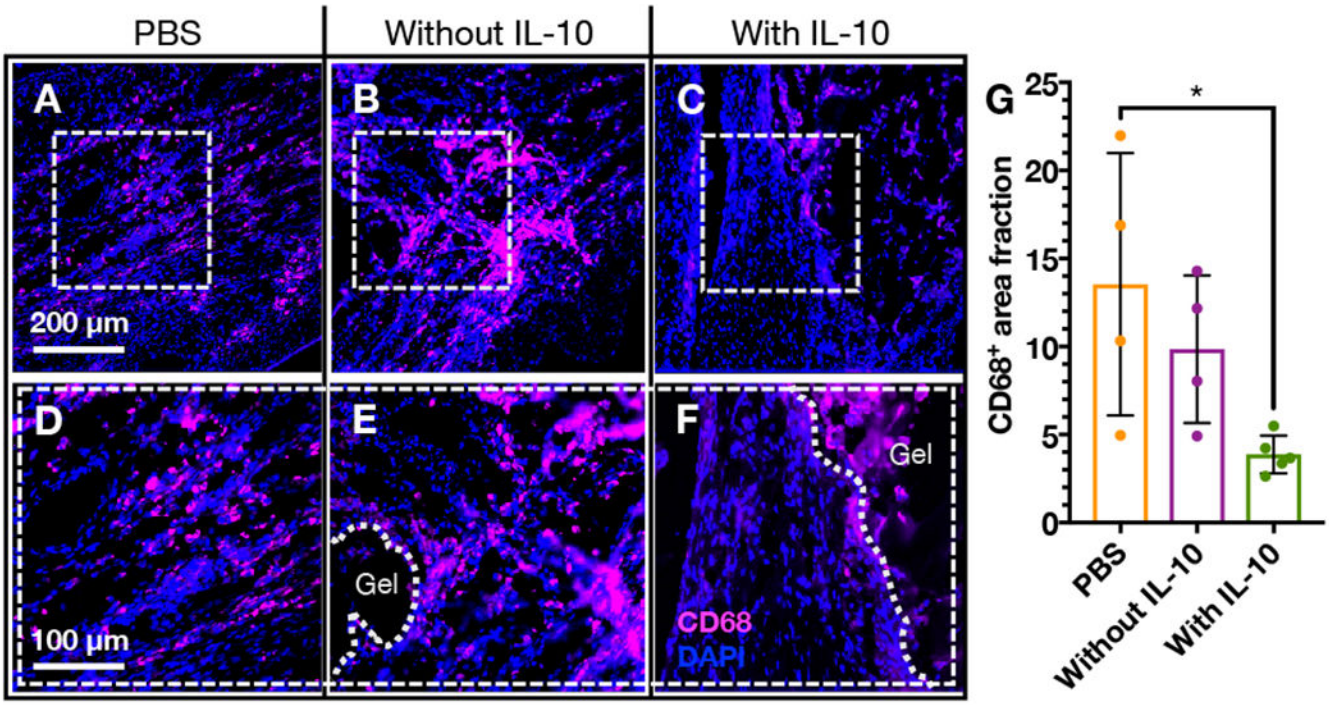

Figure 7.

A-F) Immunohistochemistry for $CD68^+$ cells (red) in the border zone and G) quantification of area fraction of cardiac tissue outside of the composite hydrogel that is $CD68^+$ after delivery of (A, D) PBS (n=4), (B, E) composites without IL-10 (n=4), or (C, F) composites with IL-10 (n=5). (mean ± SD; *$p<0.05$).

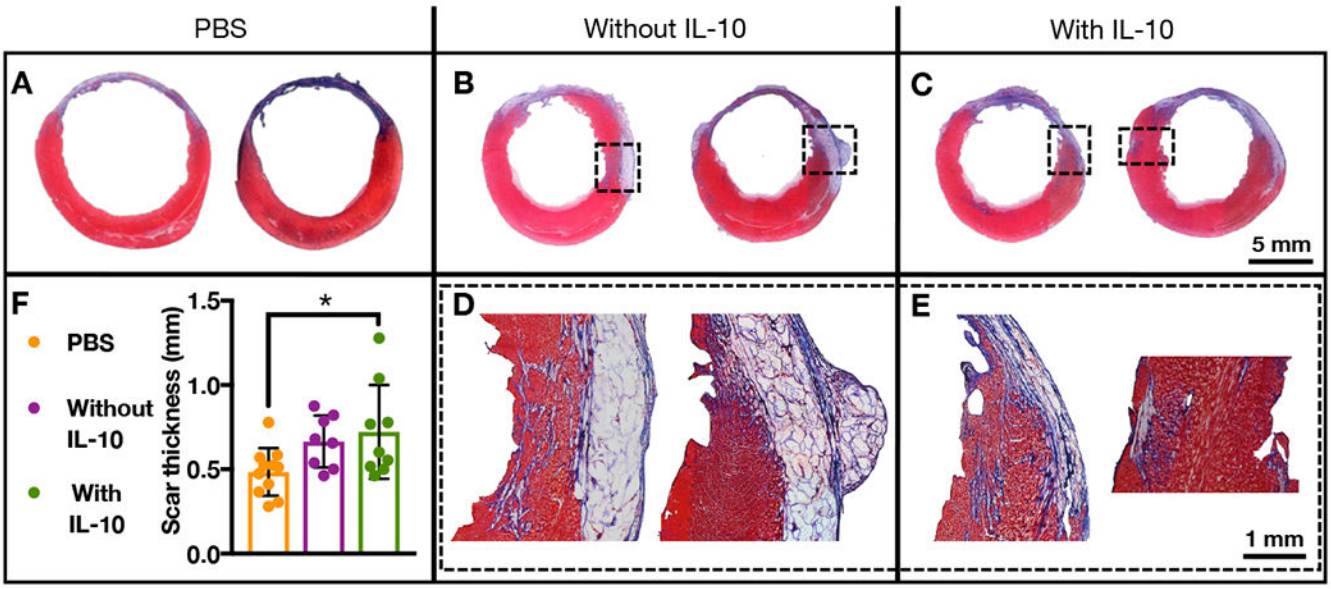

Figure 8.

(A-E) Masson's trichrome staining of cardiac tissue 28 days after delivery of PBS (n=11), composites without IL-10 (n=8), or composites with IL-10 (n=10) to rat MI. F) Quantification of scar thickness of these same treatment groups (mean ± SD; *$p<0.05$).

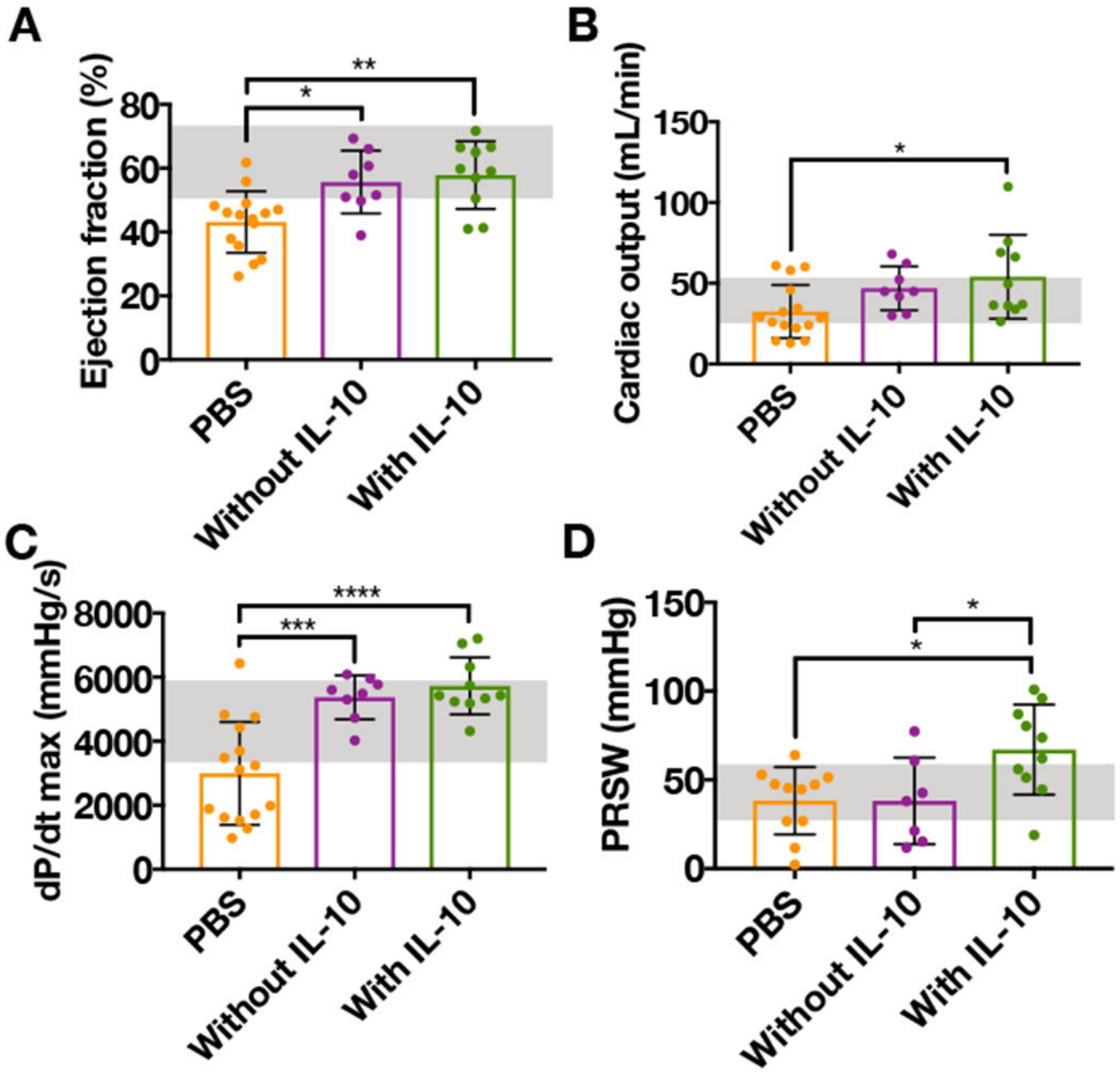

Figure 9.

A) Ejection fraction, B) cardiac output, C) dP/dT_{max}, and D) preload recruitable stroke work (PRSW) 28 days after delivery of PBS (n=15), composites without IL-10 (n=8), or composites with IL-10 (n=10) to rat MI and measured via pressure-volume catheterization (mean ± SD; *p<0.05, **p<0.01, ***p<0.001, ****p<0.0001; healthy range in shaded boxes).

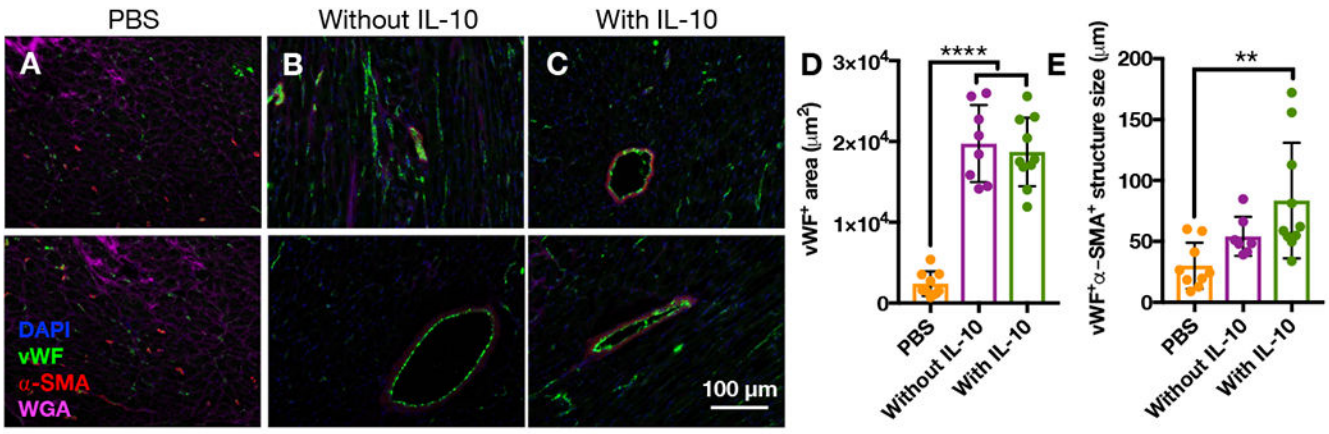

Figure 10.

Immunohistochemistry for vascular markers 28 days after delivery of A) PBS, (n=9), B) composites without IL-10 (n=8), or C) composites with IL-10 (n=10) to rat MI. Quantification of D) vWF^+ area and E) size of $vWF^+\alpha\text{-}SMA^+$ structures for these same groups (mean ± SD; *p<0.05, **p<0.01, ***p<0.001, ****p<0.0001).